
TXT-tool 1.039-1.1

Very-High Resolution Stereo Satellite Images for Landslide Mapping

Francesca Ardizzone, Federica Fiorucci,
Alessandro Cesare Mondini and Fausto Guzzetti

Abstract

Landslides are common phenomena in mountainous countries, and play an important role in the evolution of landscapes. They also represent a serious hazard in many areas of the world. Acquiring systematic information on the type, abundance, and distribution of landslides, and preparing landslide inventory maps is of fundamental importance to mitigate landslide risk. Landslide inventory maps are essential for evaluating landslide hazard, vulnerability and risk, and for studying the evolution of landscapes dominated by mass-wasting processes. Landslide maps, including geomorphological, event, seasonal, and multi-temporal inventory maps, can be prepared using different techniques. We present the results of an experiment aiming at testing the possibility of using very high resolution, stereoscopic satellite images to map rainfall-induced shallow landslides. Three landslide inventory maps were prepared for the Collazzone study area, Umbria, Italy. Two of the maps were prepared through the visual interpretation of stereoscopic satellite images, and cover the periods January–March 2010, and March–May 2010. The third inventory map shows landslides occurred in the period January–March 2010, and was obtained through reconnaissance field surveys. We describe the statistics of landslide area for the three inventories, and compare quantitatively two of the landslide maps.

Keywords

Landslide · Inventory map · Remote sensing · Satellite image · GIS

F. Ardizzone (✉) · F. Fiorucci · A.C. Mondini ·
F. Guzzetti
Consiglio Nazionale delle Ricerche, Istituto di
Ricerca per la Protezione Idrogeologica, Via della
Madonna Alta 126, 06128 Perugia, Italy
e-mail: francesca.ardizzone@irpi.cnr.it

F. Fiorucci
e-mail: federica.fiorucci@irpi.cnr.it

A.C. Mondini
e-mail: alessandro.mondini@irpi.cnr.it

F. Guzzetti
e-mail: fausto.guzzetti@irpi.cnr.it

Contents

1 Introduction	84
2 Study Area	84
3 Materials and Methods	85
3.1 VHR Stereoscopic Satellite Images	85
3.2 Hardware and Software Visualization System.....	85
3.3 Visual Interpretation Criteria.....	87
3.4 Field Surveys.....	88
3.5 Rainfall Conditions.....	88
4 Results	88
4.1 Analysis of the Landslide Inventories.....	89
5 Discussion and Conclusion	91
References	93

1 Introduction

A landslide inventory is the simplest form of landslide map (Guzzetti et al. 2000), and shows the location, the date of occurrence, and the types of mass movements that have left discernible traces in an area. A landslide map is essential for geomorphological and ecological studies, and to evaluate landslide hazard, vulnerability, and risk. Landslide maps can be classified into different types based on variable causes: geomorphological, event, seasonal, and multi-temporal inventory maps (Cardinali et al. 2001; Guzzetti et al. 2006), therefore they are traditionally prepared exploiting different techniques, such as the visual interpretation of stereoscopic aerial photographs (Bucknam et al. 2001; Cardinali et al. 2001), reconnaissance field survey (Dapporto et al. 2005; Cardinali et al. 2006; Santangelo et al. 2010), and analysis of archive information on historical landslide events (Taylor and Brabb 1986; Guzzetti 2000; Salvati et al. 2013; Devoli et al. 2007; Damm and Klose 2014; Zêzere et al. 2014; Taylor et al. 2015).

The availability of high resolution (HR) and very-high resolution (VHR) satellite images, and improved digital visualization and analysis techniques, has encouraged investigators to exploit satellite images to detect and to map landslides (e.g., Mantovani et al. 1996; Saba et al. 2010; Murillo-Garcia et al. 2015) and erosion features (Fiorucci et al. 2015). Stereoscopic and 3-dimensional (3-D) models obtained from HR and VHR images can be examined visually to detect individual landslides, or groups of

landslides, and to prepare landslide inventory maps (Alkevli and Ercanoglu 2010).

Guzzetti et al. (2012), in a recent review of the literature on landslide inventories, have shown that one of the most promising approaches exploits VHR optical, monoscopic and stereoscopic satellite images, analysed visually or through semi-automatic procedures. The authors also conclude that a combination of satellite, aerial, and terrestrial remote sensing data represents the optimal solution for landslide detection and mapping, in different physiographic, climatic, and land cover conditions.

We present the results of an experiment to test the possibility of using VHR stereoscopic satellite images, and innovative 3-D visualization technology, to prepare landslide inventory maps. The experiment was conducted in Umbria, Italy, where two inventories were prepared exploiting multiple sets of stereoscopic satellite images. A third inventory was obtained through a reconnaissance field survey conducted after a rainfall period that resulted in landslides. We measured the degree of matching between two inventories, adopting the method proposed by Carrara et al. (1992) and Ardizzone et al. (2002).

2 Study Area

The study area is in Umbria region, Italy (Fig. 1), and extends for about 90 km², including 78.9 km² of hilly terrain. Sedimentary rocks, Cretaceous to Recent in age, crop out in the area, and comprise recent fluvial deposits, continental gravel, sand and clay, travertine, layered sandstone and marl, and thinly layered limestone (Servizio Geologico Nazionale 1980). The soil texture is medium-fine, and soil thickness ranges from a few decimetres to more than one meter. Arable land, forests, urban areas, pastures, vineyards and orchards represent the land cover. Farming in the area favours the development of slope instabilities, including landslides and channelled and sheet erosion. The climate is Mediterranean, with most of the precipitation falling from October to December, and from February to May. The historical rainfall time

series (1951–2013) for the Todi rain gauge (283 m of elevation, Fig. 1) shows that the average annual rainfall is 841.1 mm, and that the maximum and minimum average monthly precipitation levels were in November (116 mm) and July (38 mm), respectively.

Landslides are abundant in the area, and are caused by meteorological triggers i.e., prolonged rainfall and rapid snowmelt events. Mass movements in the area include soil slides and flows (shallow landslides), deep-seated slides, and compound failures (Guzzetti et al. 2006; Galli et al. 2008). Shallow landslides are mainly represented and occur primarily on cultivated or abandoned areas, and are rare in the forested terrain. In the cultivated areas, mechanical ploughing and harrowing obliterate landslides features. For this reason, the lifetime of the individual shallow landslides rarely exceeds a few seasons, although reactivations and new slope failures are common where previous landslides have occurred (Fiorucci et al. 2011).

3 Materials and Methods

For the hilly portion of the study area we prepared three inventory maps using two different methods: (1) the visual interpretation of VHR stereoscopic satellite images, and (2) reconnaissance geomorphological field mapping. In this section, we first describe the satellite images, the hardware and software visualization technology, and the interpretation criteria used to prepare the landslide maps. Next, we discuss the production of the reconnaissance geomorphological field mapping, and we provide information on the rainfall history that has resulted in the many landslides.

3.1 VHR Stereoscopic Satellite Images

For our experiment, we used VHR panchromatic images taken (1) by the GeoEye-1 satellite on 12 August 2009 and on 27 May 2010, and (2) by the WorldView-1 satellite on 8 March 2010. GeoEye-1 was launched in September 2008, and

flying at an altitude of 681 km it captures images at 0.41-m panchromatic (black and white, resampled at 0.50-m) and 1.65-m multispectral (resampled at 2-m) resolution. WorldView-1 was launched in September 2007, and operating from an altitude of 496 km, it takes images at 0.50-m panchromatic and 2-m multispectral resolution. Table 1 lists the main characteristics of the stereoscopic images taken by the two satellites, and used to detect and map landslides in our study area.

Rational Polynomial Coefficients (RPCs) for the satellite images were available to us. RPCs provide a representation of the ground-to-image geometry, allowing for photogrammetric processing. We used the RPCs to generate 3-D models of each pair of stereoscopic satellite images. We estimated the accuracy of operation using eight checkpoints. Horizontal accuracy of the models, measured by the root mean square error (RMSE), was 2.2 m for the GeoEye-1 and 1.12 m for the WorldView-1 images. Vertical accuracy was 2.0 m for GeoEye-1, and 1.9 m for WorldView-1. The Bi-dimensional RMSE was 2.9 m for GeoEye-1, and 2.2 m for WorldView-1. The obtained values are within the accuracy of a 1:10,000 topographic map, and hence well suited for geomorphological and multi-temporal landslide inventory maps.

3.2 Hardware and Software Visualization System

We used ERDAS IMAGINE[®] and Leica Photogrammetry Suite (LPS) software for block orientation, and Stereo Analyst for ArcGIS[®] software for image visualization and landslide mapping. To obtain 3-D views of the VHR satellite images, we used the StereoMirrorTM hardware technology (Fig. 2).

Using Stereo Analyst for Arc ArcGIS[®], we studied the 3-D views of the topographic surface prepared with the oriented satellite images, and we collected 3-D geographical information on landslides. The software allowed the preparation of multiple sets of oriented images, all having the same reference system. To map the

Fig. 1 Location and morphology of the Collazzone study area. **a** Italy territory. Umbria region is represented by the *red polygon*. **b** Collazzone study area. The coordinate system is UTM ED50 zone 33 (EPSG 23033)

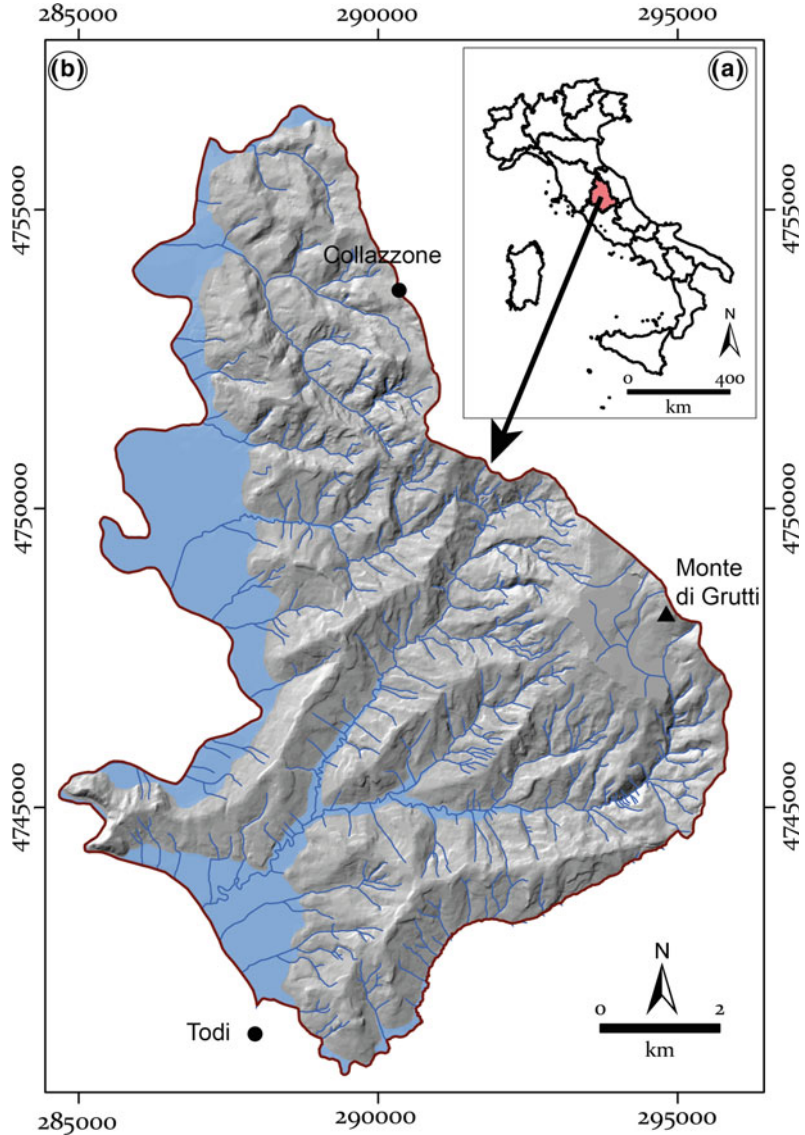


Table 1 Characteristics of the stereoscopic satellite images acquired by the GeoEye-1 and the WorldView-1 satellites, and used in our work

	Date	Overlap (%)	Azimuth angle (°)	Elevation angle (°)
GeoEye-1	12/08/2009	90	45.18	86.18
GeoEye-1	12/08/2009	90	189.90	62.3
GeoEye-1	12/08/2009	90	349.99	61.97
GeoEye-1	12/08/2009	90	244.90	13.80
WorldView-1	08/03/2010	70	77.30	57.90
WorldView-1	08/03/2010	70	141.1	52.70
GeoEye-1	27/05/2010	95	8.41	72.26
GeoEye-1	27/05/2010	95	199.51	71.99

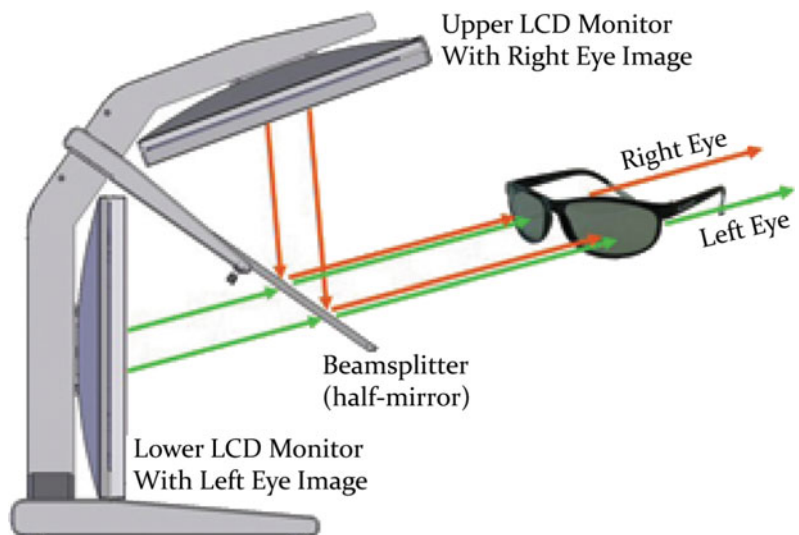
landslides in real-world 3-dimensional geographical coordinates, a 3-D floating cursor was used. When using a floating cursor, it is important that the cursor stays on the topographic surface. The software facilitates the task with an automatic terrain-following mode. A 3-D floating cursor consists of an independent cursor that is displayed on the left image and an independent cursor that is displayed on the right image of the stereo-pair. When images are not viewed in stereo, the 3-D floating cursor appears as two separate cursors. However, when viewed in stereo, the two cursors fuse to create the perception of a 3-D floating cursor. The manual adjustment of the position of the 3-D floating cursor requires the continuous attention of the operator. We used image correlation to obtain elevation information using the floating cursor (Murillo-Garcia et al. 2015). The StereoMirror™ technology allows for the 3-D visualization of large areas. For our experiment, the area covered by the GeoEye-1 stereoscopic images was $13 \text{ km} \times 17 \text{ km}$ (160 km^2), and the area covered by the WorldView-1 stereoscopic images was $24 \text{ km} \times 24 \text{ km}$ (576 km^2). The ability to analyse in 3-D multiple sets of stereoscopic images for a large area proves important for landslide mapping, chiefly for multi-temporal mapping. The hardware and software technology simplified the acquisition

of landslide information from stereoscopic images. Further, the landslide and morphological information was obtained in 3-D and stored directly in a GIS database, reducing the acquisition time and the problems (and errors) associated with the manual digitization of the landslide information and the construction of the geographical database (Galli et al. 2008).

3.3 Visual Interpretation Criteria

To recognize the landslides in the digital stereoscopic satellite images, we used the same interpretation criteria commonly adopted by geomorphologists to identify landslides on stereoscopic aerial photographs. The interpreter detects and classifies a landslide based on experience, and on the visual analysis of a set of features or characteristics that can be identified on the images (Fig. 3). These include: shape, size, tone, colour, mottling, texture, pattern of objects, and site topography (Ray 1960; Allum 1966; Rib and Liang 1978; van Zuidan 1985). Shape refers to the form of the topographic surface. Size describes the areal extent of an object. Colour, tone, mottling, and texture depend on the light reflected by the surface, and can be used to infer rock, soil and vegetation types. Mottling and texture are measures of terrain roughness and

Fig. 2 Sketch of the StereoMirror™ technology (<http://www.planar.com/>)



can be used to identify surface types and the size of debris. Pattern is the spatial arrangement of objects in a repeated or characteristic order or form. Site topography indicates the position of a place with reference to its surroundings and reflects morphometric characters. Because of the vertical exaggeration of stereoscopic vision, shape is a very useful characteristic for the identification and classification of the landslide from aerial or satellite stereoscopic images. Stereoscopic vision allows the recognition of landslides on aerial photographs or satellite images, particularly where landslides do not show evident morphological signs (Fig. 3).

3.4 Field Surveys

Following rainfall events in December 2009 (Fig. 4), we performed reconnaissance field surveys to identify and map rainfall-induced landslides in the study area. Four geomorphologists searched an area of about 90 km² in four days between January and March 2010. They drove and walked along roads, stopped where single or multiple landslides were identified, and at viewing points to check the slopes. Landslides were mapped in the field at a 1:10,000 scale, using the

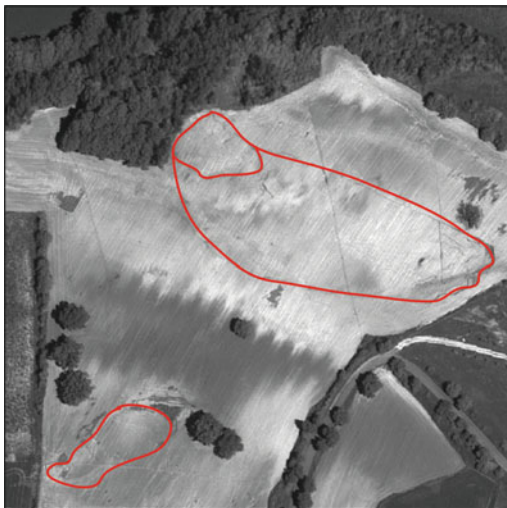


Fig. 3 Example of landslides on satellite stereo image in the Collazzone study area

geomorphological and topographic information available on site. Single and pseudo-stereoscopic colour photographs of landslides were taken with digital hand-held cameras. The cartographic and photographic information obtained in the field was used in the laboratory to map visually the individual landslides on 1:10,000 scale ortho-photographs. The landslide and morphological information was then stored digitally in a GIS database.

3.5 Rainfall Conditions

To investigate the rainfall conditions that have resulted in landslides in the study area in the period from September 2009 to May 2010, we used rainfall measurements obtained by the Todi rain gauge, located 3 km south of the study area (Fig. 1). In autumn 2009, the rain gauge measured 194 mm of rain, with 34.37 mm in four days between 14 and 17 September 2009. In the 2009–2010 winter, the rain gauge recorded 323.84 mm, with 170.86 mm in 22 days from 19 December 2009 to 9 January 2010. In the spring of 2010, the rain gauge measured a cumulated rainfall of 205 mm, with 132.34 mm in 17 days, 3–19 May 2010 (Fig. 4). Inspection of the rainfall record of Fig. 4 indicates that most of the landslides mapped in this inventory occurred presumably in the period between the end of December 2009 and the first decade of January 2010, with a second wet period in the month of May when rainfall probably caused landslides that were identified in the GeoEye image of 27 May.

4 Results

For the Collazzone hilly study area, we prepared three landslide inventory maps using the hardware and software visualization system described in Sect. 3.2, and applying the visual interpretation criteria (Sect. 3.3) to the VHR satellite images illustrated in Sect. 3.1 (Fig. 5). Two maps were obtained through the visual interpretation of VHR stereoscopic satellite images taken on 12 August 2009 and 8 March 2010 by the GeoEye-1 and the World-View-1 satellites, (MAP A), and on 27 May 2010 by the GeoEye-1

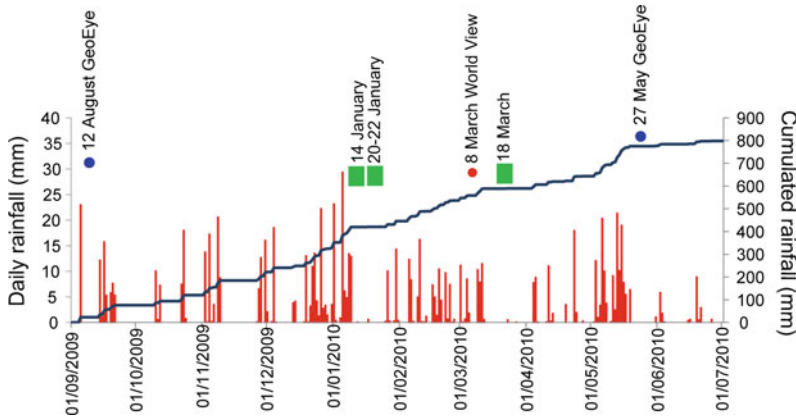


Fig. 4 Rainfall in Todi rain gauge (see Fig. 1). Rainfall conditions in the period 1 September 2009–1 July 2010. Bars show cumulated daily rainfall. Blue line shows total

cumulate rainfall. Green squares show dates of field surveys. Red dot shows date of WorldView-1 image. Blue dots show date of GeoEye-1 images (Table 1)

satellite (MAP B). The third map (MAP C) was obtained through a reconnaissance field survey conducted between 14 of January and 18 of March 2010.

To detect and map the rainfall-induced shallow landslides on 3-D digital representations of the stereoscopic satellite images, we adopted a multi-temporal approach (Fiorucci et al. 2011), and we recognized new landslides by comparing images from different dates.

To prepare MAP A (Fig. 6), we compared visually the GeoEye-1 images taken on 12 August 2009 and the World-View-1 images taken on 8 March 2010. Thus, MAP A covers the period August 2009–March 2010.

To obtain MAP B (Fig. 6), we compared visually the World-View-1 images taken on 8 March 2010 with the next images obtained on 27 May 2010 by the GeoEye-1 satellite. Therefore, MAP B covers the period March–May 2010, with most of the landslides presumably occurring in the first half of May (Fig. 4).

To obtain MAP C (Fig. 6), a reconnaissance field survey was carried out on 14, 20 and 22 January, and 18 March, 2010 with most of the landslides in the period between the end of December 2009 and the first decade of January 2010.

MAP A shows 159 shallow landslides (Fig. 6) ranging in size from 3.7×10^1 to 1.51×10^4 m², for a total landslide area $A_{LT} =$

2.94×10^5 m², that corresponds to 0.37% of the hilly portion of the study area, an average of 2.0 landslides per square kilometre (Table 2). MAP B shows 55 shallow landslides (Fig. 6), with individual landslides in the range from 2.98×10^1 to 1.16×10^4 m², for a total landslide area $A_{LT} = 8.52 \times 10^4$ m². This corresponds to 0.11% of the hilly portion of the study area, an average of 0.7 landslides per square kilometre.

The reconnaissance inventory shown in MAP C shows 76 landslides (Fig. 6), ranging in area from 4.59×10^1 to 1.89×10^4 m², for a total landslide area $A_{LT} = 1.37 \times 10^5$ m², that correspond to 0.17% of the hilly portion of the study area, and an average of 0.04 landslides per square kilometre (Table 2).

4.1 Analysis of the Landslide Inventories

We analysed the landslide inventory maps for studying the statistics of landslide area, and we compared quantitatively MAP A and MAP C that show landslides presumably occurring in the same period. For each landslide map, the planimetric area was obtained in a GIS. Table 2 lists summary statistics for the mapped landslides in the three inventories. We estimated the frequency density distribution of the landslide areas for the

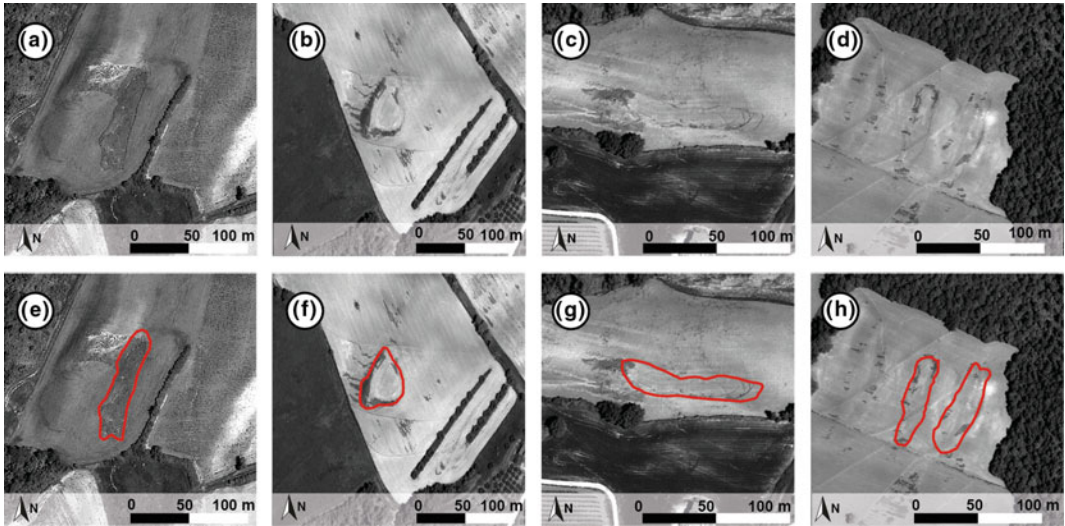


Fig. 5 Examples of landslides recognized on the GeoEye-1 satellite image taken on 27 May 2010 are shown in **a–d**. They are shown *encircled* in **e–h**, respectively

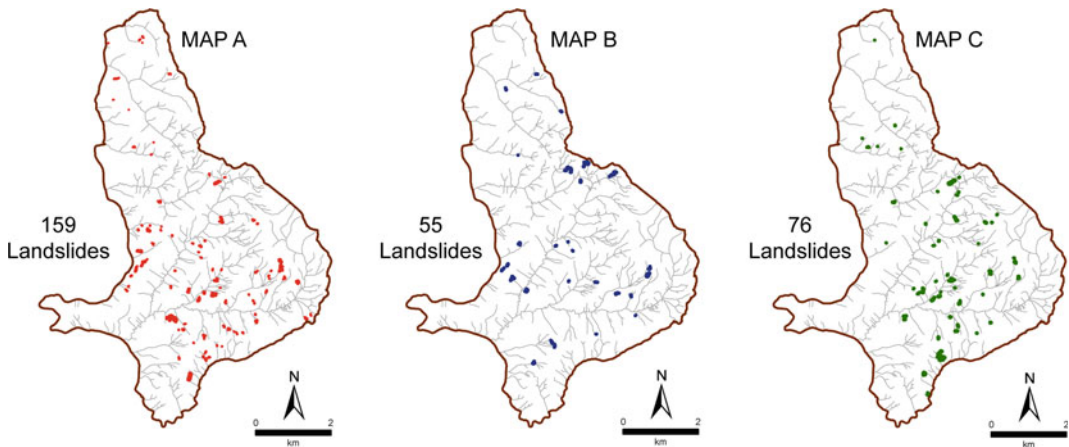


Fig. 6 Landslide inventory maps for the Collazzone study area. *MAP A* shows landslides mapped through the visual interpretation of the WorldView-1 stereoscopic images taken on 8 March 2010. *MAP B* shows landslides

mapped through the visual interpretation of the GeoEye-1 stereoscopic images taken on 27 May 2010. *MAP C* shows the landslide inventory prepared through field surveys in the period January–March 2010

three maps using the Inverse Gamma (IG) and the Double Pareto (DP) functions (Stark and Hovius 2001; Malamud et al. 2004) (Fig. 7). The two distributions provide similar results within the three inventories (Fig. 7 and Table 3), with

the standard error (ϵ in Table 3) largest for MAP B, the map with the least number of landslides. Figure 7 shows a distinct “rollover” in the Inverse Gamma distribution of landslide area for the three maps, while a problem exists

Table 2 Descriptive statistics for the three landslide inventory maps available for the Collazzone study area

	MAP A	MAP B	MAP C
Area covered (km ²)	90.0	90.0	90.0
Hilly area (km ²)	78.9	78.9	78.9
N _L (#)	159	55	76
Min A _L (m ²)	3.7 × 10 ¹	2.98 × 10 ¹	4.59 × 10 ¹
Max A _L (m ²)	1.51 × 10 ⁴	1.16 × 10 ⁴	1.89 × 10 ⁴
Mean A _L (m ²)	1.86 × 10 ³	1.55 × 10 ³	1.81 × 10 ³
Median A _L (m ²)	1.01 × 10 ³	9.78 × 10 ²	9.82 × 10 ²
St. Dev. A _L (m ²)	2.5 × 10 ³	2.05 × 10 ³	2.68 × 10 ³
A _{LT} (m ²)	2.94 × 10 ⁵	8.52 × 10 ⁴	1.37 × 10 ⁵
δ(A _L) # km ⁻²	2.0	0.7	0.04

with the estimation of the Double Pareto function for MAP B and MAP C, probably due to the limited number of landslides in these two maps.

To evaluate the geographical mismatch between MAP A and MAP C we used the Error index proposed by Carrara et al. (1992), and the corresponding Matching index proposed by Galli et al. (2008). The two indices quantify the degree of similarity between the different landslide maps, using:

$$E = \frac{(A \cup C) - (A \cap C)}{(A \cup C)} \quad 0 \leq E \leq 1 \quad (1)$$

$$M = 1 - E \quad 0 \leq M \leq 1 \quad (2)$$

We applied Eqs. (1) and (2) to the entire study area, and to the individual homologous landslides in the two inventories (MAP A and MAP C). Geographical union (\cup) and intersection (\cap) of MAP A and MAP C were obtained in a GIS. Geographical union of MAP A and MAP C was 3.73×10^5 m², and the landslide area common to both inventories was 5.89×10^4 m². The error index E was equal to 0.84, and the corresponding match index M was equal to 0.16. These values indicate a significant discrepancy between the two inventories, as indicated in Galli et al. (2008). E indices (and M indices) for individual

homologous landslides range from E = 0.35 to E = 0.90 (mean = 0.65, $\sigma = 0.15$), and M = 0.10 to M = 0.65 (mean = 0.35, $\sigma = 0.15$). The figures are similar to the values obtained by Santangelo et al. (2010) for a nearby area.

5 Discussion and Conclusion

In the literature, most of the attempts to detect and map landslides using satellite imagery (Mantovani et al. 1996; Singhroy 2005) consisted in the recognition and mapping of slope failures that have left easily recognizable morphological signs, essentially evident changes in land cover (e.g., from dense forest to exposed soil and rock). In our experiment, VHR stereoscopic satellite images were used to detect and map landslides that did not result in distinct morphological or land cover signatures that could be recognized easily using aerial photographs or field surveys. We consider the use of VHR satellite image in geographical areas where landslides are cancelled by human activity and where the signatures of failures are subtle to be an efficient tool to detect and map landslides. This is an advancement compared to previous results.

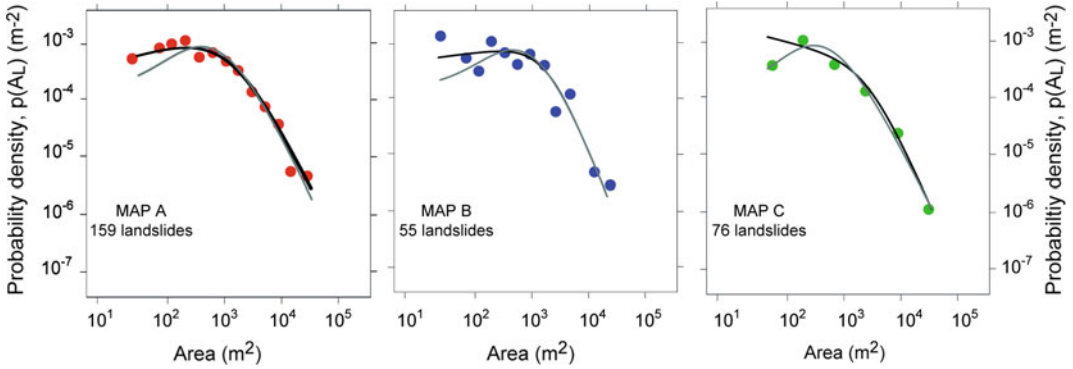


Fig. 7 Statistics of landslide size. The *graphs* show the probability density of landslide area, $p(A_L)$ for the three maps. *Coloured dots* are frequency values calculated by means of histogram estimation of logarithm of the data.

Black lines are double Pareto, and *grey lines* are inverse Gamma models of $p(A_L)$ obtained through maximum likelihood estimation

Table 3 Parameters estimated for the double Pareto (Stark and Hovius 2001) and the inverse Gamma (Malamud et al. 2004) models for the probability density of landslide area, $p(A_L)$

	IG		DP	
	$\alpha + 1$ (ε)	\bar{A}_L (m^2)	$\alpha + 1$ (ε)	\bar{A}_L
MAP A	2.45 (0.25)	325	2.24 (0.28)	201
MAP B	3.06 (0.65)	393	2.79 (0.55)	270
MAP C	2.20 (0.28)	250	2.49 (0.26)	270

The hardware and software used in the experiment allowed for the effective 3-D visualization of a large territory ($>100 \text{ km}^2$), and simplified the acquisition of 3-D landslide information and storage in a GIS database. Advantages of the system include: (i) the ability to examine a large study area, (ii) the possibility to dynamically zoom in and out and to change the image contrast during the visual inspection, facilitating the mapping of landslides of different sizes, and (iii) the ability to digitize in 3-D during the image interpretation phase, reducing the time and errors associated with the acquisition of landslide information in digital format (Galli et al. 2008).

The landslide inventory produced by visual interpretation of stereoscopic satellite images (MAP A) showed 109% more landslides, covering 114% more landslide area than the reconnaissance landslide inventory (MAP C). We attribute the difference to the possibility of recognizing slope failures in the VHR stereoscopic

images. The spatial resolution of the satellite images, $0.5 \times 0.5 \text{ m}$ for GeoEye-1 and WorldView-1, are adequate to detect and map the smallest landslides in the study area. Further, the vertical exaggeration of stereoscopic vision allowed for the detection of small (faint) morphological features related to landslides.

The area covered by the satellite stereoscopic images ($>100 \text{ km}^2$) is comparable to the area covered by small-scale aerial photographs (1:50,000 and 1:75,000), and allows the obtaining of enlargements up to 1:10,000 scale. The use of Rational Polynomial Coefficient information to generate the 3-D models allowed us to obtain accuracy levels comparable to the accuracy of 1:10,000 topographic base maps.

We estimated the probability density of landslide area $p(A_L)$ for the different landslide maps (Fig. 7 and Table 3). Inspection of the probability density curves reveals similarities in the density distribution of the landslide area, $p(A_L)$. All the empirical distributions exhibit the

same general shape, with the density for large and very large landslides obeying a negative power law trend. The Double Pareto function revealed estimation problems for MAP B and MAP C, due to the reduced number of landslides in the two maps.

The geographical mismatch between landslide maps computed using the method proposed by Carrara et al. (1992) and Ardizzone et al. (2002) revealed a discrepancy between the two inventories (MAP A and MAP C). The large error index, $E = 0.84$ depends chiefly on differences in the number of the mapped landslides in the two inventories, while the mismatch between homologous landslides is smaller, $E = 0.65$.

The experiment showed that VHR stereoscopic satellite and adequate 3-D viewing technology facilitates the production of accurate landslide inventory maps, even in areas where slope failures have left subtle signatures. This is an important step towards the systematic production of multi-temporal landslide inventories, seasonal landslide maps, and event landslide inventory maps. GeoEye-1 and WorldView-1 satellite sensors have revisiting times of only a few days (2–8 days for GeoEye-1, and 1.5–5 days for WorldView-1) allowing for the potential production of multi-temporal inventories and their rapid and frequent update. This is a mandatory step for landslide hazard and risk assessment, and for erosion and landscape evolution studies.

Acknowledgments Work conducted in the framework of the ASI MORFEO project. FF is supported by a grant of Umbria Region.

References

- Alkevli T, Ercanoglu M (2010) Assessment of ASTER satellite images in landslide inventory mapping: Yenice-Gökçebey (Western Black Sea Region, Turkey). DOI, Bull Eng Geol Environ. doi:[10.1007/s10064-011-0353-z](https://doi.org/10.1007/s10064-011-0353-z)
- Allum JAE (1966) Photogeology and regional mapping. Institute of Geological Sciences, Photogeological Unit. Pergamon Press, Oxford, p 107
- Ardizzone F, Cardinali M, Carrara A, Guzzetti F, Reichenbach P (2002) Impact of mapping errors on the reliability of landslide hazard maps. Nat Hazards Earth Syst Sci 2(1/2):3–14
- Bucknam RC, Coe JA, Chavarria MM, Godt JW, Tarr AC, Bradley LA, Rafferty S, Hancock D, Dart RL, Johnson ML (2001) Landslides triggered by Hurricane Mitch in Guatemala—inventory and discussion. U.S. Geological Survey Open File Report 01-443
- Cardinali M, Ardizzone F, Galli M, Guzzetti F, Reichenbach P (2001) Landslides triggered by rapid snow melting: the December 1996–January 1997 event in Central Italy. In: Proceedings of 1st EGS Plinius conference, 14–16 Oct 1999. Bios Publisher, Cosenza, pp 439–448
- Cardinali M, Galli M, Guzzetti F, Ardizzone F, Reichenbach P, Bartoccini P (2006) Rainfall induced landslides in December 2004 in south-western Umbria, central Italy: types, extent, damage and risk assessment. Nat Hazards Earth Syst Sci 6:237–260
- Carrara A, Cardinali M, Guzzetti F (1992) Uncertainty in assessing landslide hazard and risk. ITC J 2:172–183
- Damm B, Klose M. (2014) Landslide database for the Federal Republic of Germany: a tool for analysis of mass movement processes. In: Sassa K, Canuti P, Yin Y (eds) Landslide science for a safer geoenvironment, vol 2. Springer International Publishing, Switzerland, pp 787–792
- Dapporto S, Aleotti P, Casagli N, Polloni G (2005) Analysis of shallow failures triggered by the 14–16 November 2002 event in the Albaredo valley, Valtellina (Northern Italy). Adv Geosci 2:305–308
- Devoli G, Strauch W, Chavez G, Hoeg K (2007) A landslide database for Nicaragua: a tool for landslide-hazard management. Landslides 4(2): 163–176
- Fiorucci F, Cardinali M, Carlà R, Rossi M, Mondini AC, Santurri L, Ardizzone F, Guzzetti F (2011) Seasonal landslide mapping and estimation of landslide mobilization rates using aerial and satellite images. Geomorphology 129:59–70
- Fiorucci F, Ardizzone F, Rossi M, Torri D (2015) The use of stereoscopic satellite images to map Rills and Ephemeral Gullies. Remote Sens 7(10):14151–14178
- Galli M, Ardizzone F, Cardinali M, Guzzetti F, Reichenbach P (2008) Comparing landslide inventory maps. Geomorphology 94:268–289
- Guzzetti F (2000) Landslide fatalities and evaluation of landslide risk in Italy. Eng Geol 58:89–107
- Guzzetti F, Cardinali M, Reichenbach P, Carrara A (2000) Comparing landslide maps: a case study in the upper Tiber River Basin, Central Italy. Environ Manage 25 (3):247–363
- Guzzetti F, Galli M, Reichenbach P, Ardizzone F, Cardinali M (2006) Landslide hazard assessment in the Collazzone area, Umbria, central Italy. Nat Hazards Earth Syst Sci 6:115–131
- Guzzetti F, Mondini AC, Cardinali M, Fiorucci F, Santangelo M, Chang KT (2012) Landslide inventory maps: new tools for an old problem. Earth Sci Rev 112 (1):42–66

- Malamud BD, Turcotte DL, Guzzetti F, Reichenbach P (2004) Landslide inventories and their statistical properties. *Earth Surf Proc Land* 29:687–711
- Mantovani F, Soeters R, van Westen C (1996) Remote sensing techniques for landslide studies and hazard zonation in Europe. *Geomorphology* 15:213–225
- Murillo-Garcia FG, Alcántara-Ayala I, Ardizzone F, Cardinali M, Fiourucci F, Guzzetti F (2015) Satellite stereoscopic pair images of very high resolution: a step forward for the development of landslide inventories. *Landslides* 12(2):277–291
- Ray RG (1960) Aerial Photographs in geological interpretation and mapping. Geological survey professional paper 373, Washington, USA
- Rib HT, Liang T (1978) Recognition and identification. In: Schuster RL, Krizek RJ (eds) *Landslide analysis and control*. Transportation research board special report 176. National Academy of Sciences, Washington D.C., pp 34–80
- Saba SB, van der Meijde M, van der Werff H (2010) Spatiotemporal landslide detection for the 2005 Kashmir earthquake region. *Geomorphology* 124:17–25
- Salvati P, Marchesini I, Balducci V, Bianchi C, Guzzetti F (2013) A new digital catalogue of harmful landslides and floods in Italy. In: Margottini C, Canuti P, Sassa K (eds) *Landslide Science and practice*. Proceedings of the second world landslide forum, Rome, 19–25 Sept 2011, vol. 3, pp 409–414 (Spatial analysis and modelling)
- Santangelo M, Cardinali M, Rossi M, Mondini AC, Guzzetti F (2010) Remote landslide mapping using a laser rangefinder binocular and GPS. *Nat Hazards Earth Syst Sci* 10:2539–2546
- Servizio Geologico Nazionale (1980) *Carta Geologica dell'Umbria*. Map at 1:250,000 scale (in Italian)
- Singhroy V (2005) Remote sensing of landslides. In: Glade T, Anderson M, Crozier MJ (eds) *Landslide hazard and risk*. Wiley Press, New York, pp 469–492
- Stark CP, Hovius N (2001) The characterization of landslide size distributions. *Geophys Res Lett* 28:1091–1094
- Taylor F, Brabb EE (1986) Map showing landslides in California that have caused fatalities or at least \$1,000,000 in damages from 1906 to 1984. U.S. Geological survey miscellaneous field studies map, MF-1867
- Taylor FE, Malamud BD, Freeborough K, Demeritt D (2015) Enriching Great Britain's National landslide database by searching newspaper archives. *Geomorphology* 249:1–17
- van Zuidam RA (1985) *Aerial photo-interpretation in terrain analysis and geomorphologic mapping*. Smits Publishers, The Hague, Netherlands, ITC, p 442
- Zêzere JL, Pereira S, Tavares AO, Bateira C, Trigo RM, Quesma I, Santos PP, Santos M Verde J (2014) DISASTER: a GIS database on hydro-geomorphologic disasters in Portugal. *Nat Hazards* 72(2):503–532